scientific reports

Check for updates

OPEN

Structure-guided identification of small molecules potentially able to modulate GDF15 activity

Antonio Chiariello[1,6], Lorenzo Lenti[2,6], Lorenzo Trofarello[1], Manuela Sollazzo[3], Mattia Lauriola[1], Alberto Del Rio[2,4], Stefano Salvioli[1,5]✉, Marco Daniele Parenti[2,7] & Maria Conte[1,7]

Growth Differentiation Factor 15 (GDF15) has been associated with different pathological conditions, including cancer cachexia. Various strategies, such as monoclonal antibodies and peptide antagonists, have been developed to inhibit GDF15 activity; however, it is currently unknown whether using small organic molecules (SOMs) can effectively target GDF15. Here, we implemented a structure-based in silico screening workflow using a curated compound library to identify SOMs with potential binding affinity for GDF15. The top-ranking SOMs predicted to interact with either the monomeric or dimeric forms of GDF15 were then tested in vitro in acellular systems, as well as in normal (dermal fibroblasts, DFs) and cancer (ovarian, OV90) cells characterized by low or high GDF15 expression levels, respectively. Among the tested SOMs, dioxoimidazolidin derivative (named SOM D) emerged as particularly promising, as resulted capable of disturbing GDF15 dimer stability and GDF15-GFRAL interaction. Furthermore, SOM D significantly modulated genes and proteins recognized as downstream of GDF15 signaling, such as IL-6 and NF-κB, particularly in OV90 cells, but not in DFs. Overall, these results support the idea that GDF15 activity could be modulated through SOMs and warrant further structure–activity optimization and quantitative target-engagement studies to assess the therapeutic potential of these scaffolds as GDF15 inhibitors.

Keywords GDF15, Small organic molecules, Virtual screening, Ovarian cancer cells

Growth differentiation factor 15 (GDF15), initially described as a distant member of the transforming growth factor-β (TGF-β) superfamily, was discovered by three different research groups in 1997[1–3]. GDF15 is a stress-response molecule, expressed in different tissues, particularly in response to mitochondrial dysfunction and it can exert systemic metabolic and immunomodulatory effects also on distant tissues far from the site of production[4,5]. However, in the last years, GDF15 was found to be associated with many age-related diseases and is one of the most upregulated circulating proteins during aging[6,7].

GDF15 gene is located on chromosome 19 and encodes a 308-amino acid precursor protein (pro-GDF15) that undergoes dimerization followed by proteolytic cleavage at a conserved furine-like site (RXXR), mainly in the Golgi apparatus. This process forms the C-terminal mature GDF15 dimer (m-GDF15), which represents the predominant secreted form[8,9]. Despite the extensive research, the precise mechanism of GDF15 action is not completely understood. The only certain specific receptor identified for GDF15 is the GDNF α-like receptor (GFRAL) that requires the action of the co-receptor REarranged during Transfection (RET). While RET is widely expressed across different tissues, GFRAL expression is believed to be restricted to neurons of the nucleus of the solitary tract (NST) and the area postrema (AP), two adjacent structures in the dorsal vagal complex of the hindbrain[10–13], although lower levels have been observed also in peripheral tissues, like testis and adipose tissue, and certain cancers[14]. The interaction of GDF15 with GFRAL and RET modulates different signaling pathways, including NF-κB, ERK1/2, Akt, FOS, and PLC-γ[15,16]. The main biological activities of the GDF15-GFRAL axis include the regulation of body weight and the reduction of food intake[17]. Moreover, GDF15 can also act on

[1]Department of Medical and Surgical Sciences (DIMEC), University of Bologna, 40126 Bologna, Italy. [2]Institute for Organic Synthesis and Photoreactivity (ISOF), National Research Council of Italy (CNR), Bologna, Italy. [3]Department of Pharmacy and Biotechnology (FABIT), University of Bologna, 40126 Bologna, Italy. [4]Innovamol Srl, Strada San Faustino 167, Modena, Italy. [5]IRCCS Azienda Ospedaliero-Universitaria Di Bologna, Bologna, Italy. [6]Antonio Chiariello and Lorenzo Lenti have contributed equally to this work. [7]Marco Daniele Parenti and Maria Conte have contributed equally to this work. ✉email: stefano.salvioli@unibo.it

peripheral tissues by increasing lipolysis and oxidative metabolism[5]. Notably, several actions of GDF15 appear to be independent of central GFRAL signaling, suggesting alternative or context-dependent mechanisms of action.

GDF15 has also been implicated in the regulation of inflammatory processes[18]. Different studies showed a possible pro-inflammatory role for GDF15 through an up-regulation of interleukin-6 (IL-6)[19,20]. Furthermore, GDF15 is also considered as a member of the senescence-associated secretory phenotype (SASP)[21] and a role in cell cycle regulation has been proposed. It has been observed that GDF15 treatment increased cell proliferation of human umbilical vein endothelial cells (HUVECs) by enhancing the expression of G1 cyclins, cyclins D1 and E, through the PI3K/Akt, ERK, and JNK pathways[22].

GDF15 has been associated with several pathological conditions, including type 2 diabetes, sarcopenia, cardiovascular diseases, hypertension, neurodegenerative diseases, renal dysfunctions, and cancer[8]. For instance, we found a higher protein expression of m-GDF15 in the brain of Alzheimer's patients as well as higher plasma level in patients with muscle atrophy, compared to controls[23,24]. Moreover, an association of GDF15 levels with frailty and overall survival has been observed[7,8,25]. In the context of cancer, GDF15 has been associated with tumor progression, migration and invasiveness, although its role appears to be highly context-dependent[26]. However, GDF15 plasma levels are found elevated in cancer patients, supporting its potential role as both a biomarker and a therapeutic target across different types of cancer[17]. Finally, the role of GDF15 in inducing cancer cachexia is well established. Different studies in mice have shown that GDF15 mediates cancer cachexia, leading to weight loss, lean and fat mass loss, reduced food intake and cachexia, through the GDF15-GFRAL axis[17]. A recent study showed that GDF15 determined weight loss by increasing energy expenditure in muscles[27]. All the findings on GDF15-cancer relations increased the interest in developing pharmacological inhibitors targeting GDF15 or its receptor GFRAL. In this context, inhibition of the GDF15-GFRAL axis could represent a promising strategy to alleviate cancer cachexia and anorexia symptoms. For example, a phase 2 clinical trial for ponsegromab, a GDF15-blocking antibody, showed that patients with cancer cachexia had increased weight gain as well as improved appetite and physical activity following 12 weeks of treatment[28]. Moreover, GDF15 inhibition has been proposed as a strategy to enhance the efficacy of cancer immunotherapy by mitigating resistance mechanisms[29]. However, monoclonal antibodies have limitations, such as high costs, limited tissue penetration, safety concerns and less modularity of the effect. Recent studies have also reported peptide-based inhibitors targeting the GDF15/GFRAL axis. One investigation described C-terminal fragments of GDF15 which bound the GFRAL extracellular domain and inhibited receptor signaling in the micromolar range[30]. Another work developed a 29-residue peptide antagonist ("GRASP") of the GFRAL–RET complex, that bound GFRAL and attenuated GDF15- and cisplatin-induced anorexia in vivo[31]. More recently, an article described bicyclic tandem peptides derived by phage-display and structure-guided design to mimic the GDF15 homodimer and inhibit signaling via the GDF15–GFRAL–RET complex[32]. Although these peptidic inhibitors provide important proof-of-concept for antagonizing the GDF15–GFRAL interaction, a small-molecule inhibitor may offer several advantages, such as improved oral bioavailability, enhanced tissue penetration (including potential access to the central nervous system where GFRAL is expressed), greater metabolic stability, simpler manufacturing and formulation, and the ability to cross cell membranes or modulate allosteric sites rather than simply competing at the large surface protein–protein interface of the ligand–receptor. Thus, a well-designed small-molecule binder of GDF15 (or GDF15–GFRAL interface) could provide a more drug-like profile for therapeutic development. In this study, we pursued an early-stage, structure-guided probe-discovery strategy to identify small organic molecules (SOMs) capable of interacting with GDF15. Using an in silico screening approach applied to a curated library of commercially available compounds, we selected the six top-ranking SOMs and tested their in vitro effects in both acellular system and normal and cancer human cells, in order to verify whether any of them were actually capable of inhibiting the action of GDF15. Our results suggest that the dioxoimidazolidin derivative named SOM D seems to be the most promising for further testing.

Materials and methods

Protein structure preparation

The crystallographic structure of human Growth Differentiation Factor 15 (GDF15) was retrieved from the RCSB Protein Data Bank (PDB Code 5VT2). Two biologically relevant oligomeric states were considered: monomeric and dimeric GDF15. Since no experimental evidence was available regarding putative receptor-binding sites of GDF15 in both single-chain and dimeric forms of GDF15, to define the most plausible binding regions distinct approaches were employed for the monomeric and dimeric protein forms. For the monomeric GDF15, the putative site was selected based on intramolecular recognition features inferred from the protein's own secondary structure. Specifically, a short peptide fragment corresponding to residues 57–60 of the GDF15 sequence was used as a structural reference to locate the interaction region between the two monomers and therefore used to define the docking grid box for subsequent virtual screening. For the dimeric GDF15, the putative site was identified using P2Rank server[33], a machine learning-based pocket prediction algorithm that evaluates geometric and physicochemical properties of the protein surface. The highest-ranked predicted pocket, located at the interface region between the two monomeric subunits, was selected for docking grid definition.

All protein structures were prepared using protein preparation workflow as included in the software package Maestro (Schrödinger Release 2024-2: Protein Preparation Workflow; Epik, Schrödinger, LLC, New York, NY, 2024; Impact, Schrödinger, LLC, New York, NY; Prime, Schrödinger, LLC, New York, NY, 2025). The preparation included removal of all crystallographic water molecules and heteroatoms not involved in ligand binding, correction of incomplete side chains, and addition of polar hydrogen atoms, as well as assignment of correct protonation states at pH 7.4.

Ligand library preparation

The Hit Locator Library from Enamine (https://enamine.net/compound-libraries/diversity-libraries/hit-locator-library-460) was used for screening. Structures were downloaded in SDF format and converted to 3D conformers using Open Babel. Each ligand was subjected to energy minimization with the MMFF94 force field and assigned Gasteiger partial charges. To ensure a uniform and relevant screening set, duplicates, reactive compounds, and unstable species were filtered out using RDKit. The final ligand library contained approximately 460 K unique structures, all stored in PDBQT format compatible with AutoDock Vina.

Docking protocol

Molecular docking was performed using AutoDock Vina v1.2.7[34,35] on both monomeric and dimeric GDF15 models. Docking grids were centered on the putative binding pocket identified as described above. The grid dimensions were adjusted to fully encompass the binding site, with spacing set to 1.0 Å. For each ligand, up to 20 poses were generated, and the best-scoring conformations were selected according to the Vina scoring function (an empirical estimate of binding free energy). Docking simulations were executed on a high-performance Linux environment using multicore parallelization to increase throughput.

Post-docking analysis

For the 50 top-ranked compounds obtained from the docking, the residues predicted to interact with each ligand (based on the best-scoring binding pose) were extracted and tabulated in a binary interaction matrix. In this matrix, columns correspond to individual GDF15 dimer residues, while rows represent ligands, with each cell indicating the presence or absence of an interaction between a residue and a given compound. To evaluate the diversity of binding profiles, pairwise similarity between ligands was calculated using an asymmetric similarity metric defined as the proportion of residues with positive interaction values in the reference ligand that were also contacted by the compared ligand. This measure, computed across all 18 residues, quantifies the degree to which the interaction pattern of one compound is encompassed by another. By applying this criterion, the compounds displaying the most distinct interaction profiles were identified, ensuring maximal structural and functional diversity among the selected candidates.

Compound source

Selected molecules were purchased in milligram quantities from Enamine. Purity of compounds was ≥ 95%, as declared by the chemical vendor.

Analysis of SOMs specificity for GDF15

The capability of the SOMs to bind and disrupt GDF15 dimeric form was first tested in an acellular system through a western blotting analysis. Briefly, 50 ng of purified human recombinant GDF15 (G3046, Sigma) were incubated with each SOM at 200 µM or vehicle (DMSO) for 30 min at 4 °C, in slow agitation. Then, samples were cross-linked to preserve the dimeric form of GDF15, by adding glutaraldehyde in PBS at a final concentration of 0.5%, for 45 min at 4 °C, prepared for SDS-PAGE and western blotting was performed, as indicated in section "Protein extraction and western blotting analysis". GDF15 antibody was used to visualize the monomeric and dimeric form of GDF15.

Interference with GFRAL receptor was tested by using the GDF15:GFRAL [Biotinylated] Inhibitor Screening Chemiluminescent Assay Kit (82875, BPS Bioscience). SOMs were tested at 200 µM, following manufacturer's instructions, and chemiluminescence was read using Glomax Discover (Promega, USA). Purified human recombinant GDF15 (G3046, Sigma) was used as negative control.

Cell cultures, *Gdf15* in vitro knock down (KD) and treatments

To investigate the potential biological effects of SOMs, two cellular models were used, namely commercially available primary Dermal Fibroblasts (DFs) (Cti biotech), obtained from 2 young donors (age range 24–30 years), and OV90 cell line, derived from ovary papillary serous adenocarcinoma, selected among a number of other models on the basis of the basal levels of GDF15 they produced. GDF15 protein levels were assessed in culture supernatants by ELLA assay. Based on this screening, DFs and OV90 cells were selected as representative models for subsequent experiments (see Results section).

Both DFs and OV90 were cultured in high glucose DMEM supplemented with 10% heat-inactivated fetal calf serum (FCS), penicillin (100 units/ml), streptomycin (100 µg/ml), and 2 mM L-glutamine (all from Sigma), in an incubator at 5% CO_2, with a humidified atmosphere of 37 °C. The DFs used for the experiments were between the 8th and 12th passages.

GDF15 KD on OV90 was achieved using RNA interference (RNAi) strategy. Small interfering RNA (siRNA) targeting GDF15 and scramble siRNA (negative control) were purchased from Cohesion Biosciences. A specific combination of siRNA against GDF15 was selected after testing the silencing efficacy of different combinations of three different siRNA. Transfections were performed using ScreenFect siRNA reagent (ScreenFect GmbH), following manufacturer's indications. Briefly, 70,000 cells were seeded in a 12-wells plate and scramble or GDF15 siRNA were mixed to transfection reagent, incubated at room temperature for 20 min and then added to the cells. Medium was replaced after 24 h with fresh complete medium. Cells were harvested after a further 72 h for RNA extraction.

The SOMs were resuspended in DMSO to make a stock solution of 50 mM. A working solution of 1 mM was obtained from the stock by diluting it in fresh complete DMEM. Treatments were performed in 24-well plates by seeding 35,000 cells/well. SOMs were added to the cells the day after seeding at a final concentration of 100 µM. At the end of the treatment (24, 48 or 72 h) cells were harvested, and viability and proliferation were evaluated

with the Cell Drop FL cell counter (DeNovix) after staining with Trypan blue dye. Cells were then frozen at -80 °C until RNA or protein extraction.

Ella automated immunoassay system

The supernatant level of GDF15 was analyzed using the Simple Plex Human Cartridges (ProteinSimple/ Bio-Techne) run on an Ella Automated Immunoassay System (ProteinSimple/ Bio- Techne), according to manufacturer's instructions.

RNA extraction and Real Time RT-PCR analysis

Total RNA was extracted from DFs and OV90 pellets using the EasyPure RNA kit (TransGen Biotech Co.). RNA quantification and purity analysis were performed using NanoDrop One Spectrophotometer (Thermo Scientific). cDNA synthesis was performed with HIScript III RT SuperMix for qPCR (+ gDNA wiper) (Vazyme Biotech).

Gene expression was analyzed by Real Time RT-PCR, performed using SsoAdvanced Universal SYBR Green Supermix (Bio-Rad) and a Rotor gene Q 6000 system (Qiagen). A relative quantification was obtained using *Gapdh* as reference gene. The relative expression ratio was obtained using the $2^{-\Delta\Delta CT}$ method. All the primers used in this study were predesigned and pre-validated and purchased from Bio-Rad. More information about primers is available at www.bio-rad.com/PrimePCR.

Protein extraction and western blotting analysis

Protein extraction from OV90 cells was performed using RIPA buffer with the following composition: Tris HCl pH 8 50 mM, NaCl 150 mM, Sodium deoxycholate 0.5%, SDS 0.1% and Triton X-100 1%. Protease and phosphatase inhibitors (Sigma) were added to the lysis buffer. Pellets were resuspended in the buffer by vigorous pipetting, left on ice for 15 min, vortexing few times. Lysates were then centrifuged at 15,000 rpm at 4 °C for 15 min and the supernatants were collected. Bradford's method was performed for quantification, and protein extracts were then stored at -80 °C until used.

Protein expression was then analyzed by western blotting. 20 µg of proteins were separated on a 4–15% Mini-PROTEAN® TGX™ Precast Protein Gels (Bio-Rad), transferred on a PVDF membrane (Trans-Blot transfer, Bio-Rad) and then immunoblotted with the appropriate primary antibody. GAPDH was used as loading control. Chemidoc system (Bio-Rad) was used for acquisition. Densitometric analyses of western blotting bands were performed using the Fiji software. Primary antibodies and dilutions used are listed in Table 1.

Glucose consumption and ROS production analyses

Glucose consumption and ROS production were analyzed in OV90 cells, using commercially available kits. Specifically, Glucose-Glo™ Assay was used for glucose measurement in the culture media and ROS-Glo™ H_2O_2 Assay for ROS measurement. Both kits were purchased from Promega.

Briefly, for glucose measurement, 8000 cells/well were seeded in a 96-well plate. After 72 h of treatment with 100 µM of SOMs, an aliquot of the culture medium was taken and diluted to 1:300 in PBS. Glucose concentration was then quantified. In particular, the assay couples glucose oxidation and NADH production with a bioluminescent NADH detection system. Glucose dehydrogenase uses glucose and NAD+ to produce NADH. In the presence of NADH a pro-luciferin Reductase Substrate is converted by Reductase to luciferin that is then used by Ultra-Glo™ Recombinant Luciferase to produce light.

For ROS production measurement, 8000 cells/well were seeded in a 96-well plate. Cells were treated with 100 µM of the SOMs for 72 h. The kit uses a substrate that reacts with H_2O_2 to create a luciferin precursor. This precursor is then converted to luciferin that is then used by Ultra-Glo™ Recombinant Luciferase to produce light. Light signal is proportional to the amount of H_2O_2 in the sample.

All treatments were performed in triplicate, in two independent experiments pooled together, and chemiluminescence was assessed using the GloMax multiplate reader (Promega).

Primary antibody and catalog number	Dilution used	Supplier
GDF15 (#ab206414)	1:1000	Abcam
NF-κB P65 (#4764)	1:1000	Cell Signaling
NF-κB P65-P^{Ser536} (#3033)	1:1000	Cell Signaling
VDAC (#4661)	1:1000	Cell Signaling
Grp78 (#3177)	1:1000	Cell Signaling
Ndufs1 (#70264)	1:1000	Cell Signaling
Sdha (#11998)	1:1000	Cell Signaling
Uqcrc2 (#99258)	1:1000	Cell Signaling
Cox IV (#4850)	1:1000	Cell Signaling
GAPDH (NB300-327)	1:10,000	Novus Biological

Table 1. List of primary antibodies used.

Statistical analyses

Results are shown as mean ± standard deviation (SD). The Shapiro–Wilk normality test was performed to check whether the data were normally distributed. Then, Student's t test was used to analyze the mean values after each treatment with respect to the controls. SPSS 23.0 software for Windows (SPSS Inc.; Chicago, IL, USA) was used for analyses. P values < 0.05 were considered statistically significant.

Results

In silico screening allows the identification of potential GDF15-interacting SOMs

To identify novel SOMs potentially capable of interacting with GDF15, a structure-based virtual screening workflow was implemented. The approach combined the consideration of distinct GDF15 states, and systematic molecular docking of a curated compound library. Since GDF15 can exist in both monomeric and dimeric forms, both structural states were included in the screening pipeline. This dual approach allowed exploration of distinct binding site topologies potentially involved in ligand recognition, improving the likelihood of identifying modulators that could stabilize or disrupt specific conformations of the protein. Each form was independently subjected to docking grid generation around the putative interaction surfaces. A large library of commercially available SOMs was then docked into both structural states, SOMs were ranked according to docking scores, and the most promising candidates were selected based on both predicted binding affinity and interaction profile diversity, ensuring prioritization of chemically and functionally diverse scaffolds for subsequent in vitro analyses. Finally, sample availability from compound provider was also verified, leading to a final list of 6 top-ranking SOMs, 3 for each of the different state of the target considered in the study, that were purchased and experimentally tested. Selection of the six SOMs balanced (i) top docking rank (Vina score), (ii) removal of duplicates/reactive/unstable structures, (iii) diversity of predicted residue-contact 'interaction fingerprints' within the target pocket, and (iv) commercial availability. List of selected SOMs is reported in Table 2, while docking scores and key interacting residues for the final six SOMs are reported in Suppl. Table 1.

All tested SOMs reduce the apparent abundance of GDF15 dimer band while SOM C, D, E and F also reduce GDF15-GFRAL binding

First, we tested in an acellular system the ability of the selected SOMs to reduce the abundance of the dimeric form of GDF15, considered the biologically most active form of this protein. After incubating 50 ng of human recombinant GDF15 protein with the SOMs (200 μM), we performed a western blotting analysis to evaluate the relative abundance of the dimeric and monomeric forms of GDF15. Incubation of recombinant human GDF15 with each SOM decreased the intensity of the disulfide-linked dimer band compared to the vehicle control, suggesting that all SOMs interact with regions critical for dimer stability (Fig. 1A and B). Statistical significance was reached for all SOMs except SOM C, indicating that, although all compounds show a trend toward destabilizing the dimer, their efficacy differs, with SOM C displaying a weaker or more variable effect. We then sought to analyze the binding of GDF15 to GFRAL upon SOM treatment. To do so, we used a commercial chemiluminescent assay, which uses streptavidin-HRP to detect biotin-labeled GFRAL, that binds to GDF15-coated wells. In such a purified-protein format, SOM C, D, E and F moderately but significantly reduced GDF15–GFRAL interaction relative to vehicle and to SOMs A and B, supporting a direct modulation of the GDF15–GFRAL interaction under these conditions (Fig. 1C). The absence of a marked effect for SOMs A and B implies either binding outside the receptor interface or insufficient affinity to perturb GDF15–GFRAL association under the assay conditions. In particular, SOMs D, E and F were originally identified through virtual screening against the dimeric form of GDF15, and their ability to impair GDF15–GFRAL interaction can be explained by considering the location of the predicted binding site. Figure 1D illustrates as an example the predicted binding mode of two molecules (D and E) within the interfacial cavity of the GDF15 dimer; both ligands occupy overlapping regions at the dimer interface, forming a dense network of hydrogen bonds and hydrophobic contacts with residues critical for structural stabilization. Interestingly, due to the symmetry of the active site cavity, the two ligands are predicted to form key interaction with the same residues but in different GDF15 subunits, such as the hydrogen bond interactions with Cys48 and Cys78, and the pi-pi interactions, in parallel or T-shaped geometries, with His66. The positioning of both molecules along the inter-monomer cleft suggests that they could act by perturbing the local geometry of this interface, thereby potentially modulating the relative orientation of the two subunits.

Effect of SOMs on viability and proliferation of OV90 cells and DFs

To evaluate the potential biological effects of SOMs in vitro, two different cell models were selected, namely normal primary DFs and OV90 ovarian cancer cell line. These cellular models were chosen among others (including HK2, UOK, K562, NTHY and TPC1 cell lines) based on their markedly different levels of GDF15 production, as determined by ELLA analysis of cell culture supernatants. Specifically, OV90 cells exhibited the highest levels of secreted GDF15, whereas DFs showed the lowest levels (Suppl. Figure 1A). This difference between DFs and OV90 was further confirmed at the mRNA level by real-time RT–PCR analysis (Suppl. Figure 1B), in particular, OV90 cells showed a much higher expression of *Gdf15* than DFs.

We first performed proliferation and viability tests in a 72 h-time course in OV90 cells, assessing both cell viability and total cell number upon treatment with each SOM at 100 μM. At 24 and 48 h, no evident effects were observed, except for SOM E, which significantly reduced both viability and proliferation, compared to control (Fig. 2 A, B). This effect was even more evident at 72 h; at this time point, also SOMs C, D and F reduced the total number of cells, compared to controls, although the effect of SOM C was not statistically significant (Fig. 2B). In DFs, after a 72 h-treatment, no significant effects were observed, except for SOM E that tended to reduce viability (Fig. 2C, D).

Name	Vendor ID	Chemical structure	Predicted binding site
A	Z217241126	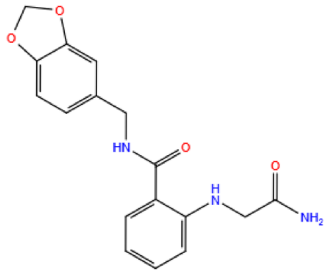	Monomer
B	Z977892838	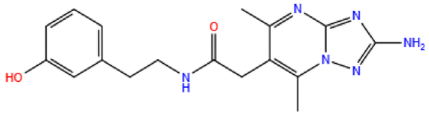	Monomer
C	Z356234358	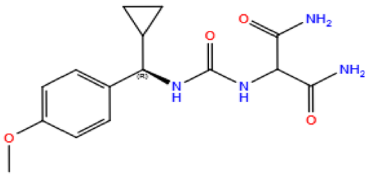	Monomer
D	Z771945868	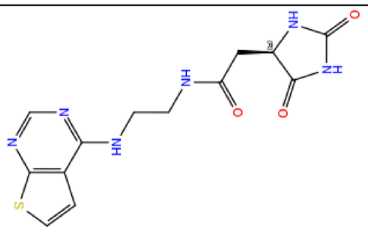	Dimer
E	Z79498276	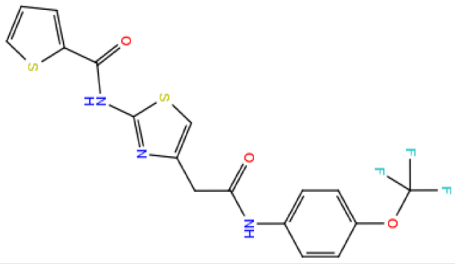	Dimer
F	Z55806982	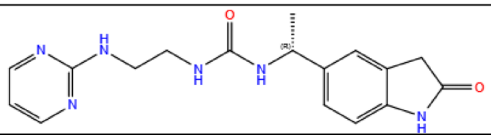	Dimer

Table 2. List of selected SOMs and their chemical structure.

Since SOMs A and B seemed not to decrease GDF15-GFRAL interaction nor affect proliferation and viability, they were discarded from further analyses. SOM E was further tested for mitochondrial respiration on OV90 cells and caused an immediate drop in oxygen consumption even at 50 µM dose (Suppl. Figure 2), suggesting potential off-target effects, and it was therefore excluded from subsequent analyses.

Modulation of gene expression is mostly observed in OV90 cells upon SOM D treatment

To investigate the possible effects of SOMs C, D and F on gene expression, we performed quantitative real time RT-PCR analyses on RNA extracted from both cell lines treated with 100 µM of the selected SOMs for 72 h. First, we evaluated the expression of genes related to cell cycle and proliferation. *p21* expression was significantly higher in OV90 cells treated with SOM C and D, compared to DMSO-treated control cells (Fig. 3A). In DFs, no significant differences were observed (Fig. 3B). *Ki67* expression was reduced by SOM D treatment in both OV90 (Fig. 3C) and DFs (Fig. 3D).

We next analyzed the expression of *p53* and *Bax*, two genes involved in apoptosis. Notably, p53 is also a GDF15 transcription factor[9,36]. *p53* expression was reduced in OV90 cells treated with SOM C and SOM D

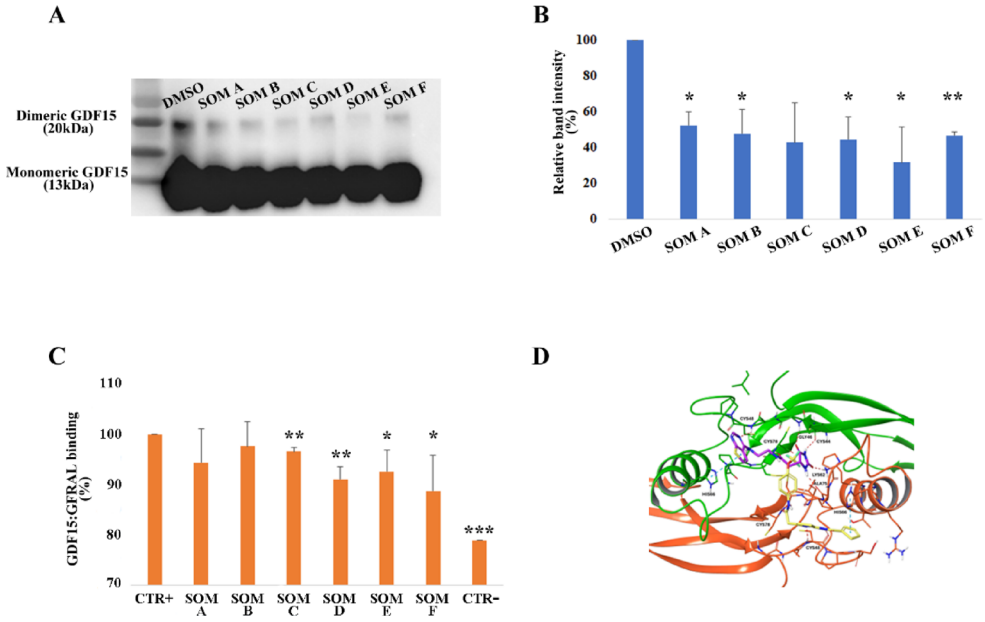

Fig. 1. Analysis of small organic molecules (SOMs) specificity for GDF15. (**A**) Representative western blotting analysis of human recombinant GDF15 (50 ng), incubated with each SOM (200 µM) or the solvent (DMSO), for 30 min. Both dimeric and monomeric forms of GDF15 are visible. (**B**) Relative band intensity of dimeric GDF15. Data are shown as relative intensity normalized to vehicle (DMSO). Densitometric quantification was performed using Fiji software. (**C**) Chemiluminescence assay, testing the ability of SOMs to disrupt GDF15-GFRAL binding. Data represent the percentage of GDF15–GFRAL binding relative to the positive control (no inhibitors). (**D**) Predicted binding mode of compounds D (purple) and E (yellow). The two GDF15 monomers are colored respectively green and orange, interacting residues are drawn as thick tubes and labeled. Hydrogen bonds are represented as red dotted lines, pi-pi interactions as blue dotted lines. Three independent experiments were performed. Data are expressed as mean ± SD. Student's t-test was applied. $*p < 0.05$, $**p < 0.01$.

(Fig. 3E). In DFs, SOM F determined a not significant increase in *p53* expression (Fig. 3F). As regards *Bax* expression, SOM D reduced its expression in OV90 cells (Fig. 3G). In DFs, SOM F determined a similar trend to that observed for *p53* (Fig. 3H).

We then evaluated the expression level of *Gdf15* itself and *Akt*, a molecule involved in the GDF15 signaling pathway[15]. In OV90 cells, SOM D caused a reduction in the expression of both *Gdf15* and *Akt* (Fig. 3I, K), while in DFs no significant variations were observed (Fig. 3J, L). Since it is unclear whether GDF15 directly regulates the expression of Akt, we sought to determine whether the effect of SOM D was mediated by GDF15 downregulation. To this end, we performed the same analysis upon a RNAi on OV90 cells, using a siRNA targeting GDF15. About 70% of *Gdf15* expression was effectively reduced by siRNA treatment (Suppl. Figure 3A) and, similarly to what was observed with SOM D, GDF15 silencing caused a reduction in *Akt* expression, as well as *Ki67* (Suppl. Figure 3B, C).

To further assess whether the tested SOMs can actually impinge upon the expression of genes involved in GDF15 signaling pathways, we investigated the expression of some recognized targets of GDF15 activity. In particular, GDF15 is strongly associated with mitochondrial stress, with reported mitochondria-protective effects. Moreover, both pro- and anti-inflammatory effects have been associated with GDF15[5,9,19,20]. Therefore, we evaluated the expression of *Pgc1α*, a gene involved in mitochondrial biogenesis, and *Il6*, an inflammation-associated cytokine, both reported to be modulated by GDF15[20,37]. *Pgc1α* expression was significantly reduced by SOM D treatment in OV90 (Fig. 3M), while no significant variations were observed in DFs (Fig. 3N). Similarly, *Il6* expression was reduced in OV90 after SOM D treatment (Fig. 3O) and no significant differences were found in DFs (Fig. 3P). Overall, these data suggest that SOM D may exert biological effects consistent with at least a partial GDF15 inhibition. Interestingly, these effects were observed in OV90, which display high basal levels of *Gdf15* expression and its protein secretion (see Suppl Fig. 1) but not in DFs which are characterized by low basal GDF15 levels. To further support this hypothesis, another downstream target of GDF15 was analyzed, *i.e.*, the activation of NF-κB transcription factor. It is reported that GDF15 suppresses NF-κB activity[16]. In line with this, we evaluated the phosphorylation of the p65 subunit at Ser536, a well-established marker of NF-κB activation. Consistently, the ratio between the total p65 and its phosphorylated form (at Serine 536) was significantly increased upon treatment with SOM D and SOM F (Fig. 4). This finding supports the hypothesis that these SOMs, particularly SOM D and SOM F, may act as partial inhibitors of GDF15 signaling.

SOM D determines an alteration of mitochondrial proteins expression

We further characterized the biological effects of SOMs by specifically testing whether these treatments induced stress at endoplasmic reticulum or mitochondrial level, thus impinging upon GDF15 processing. To this end, we

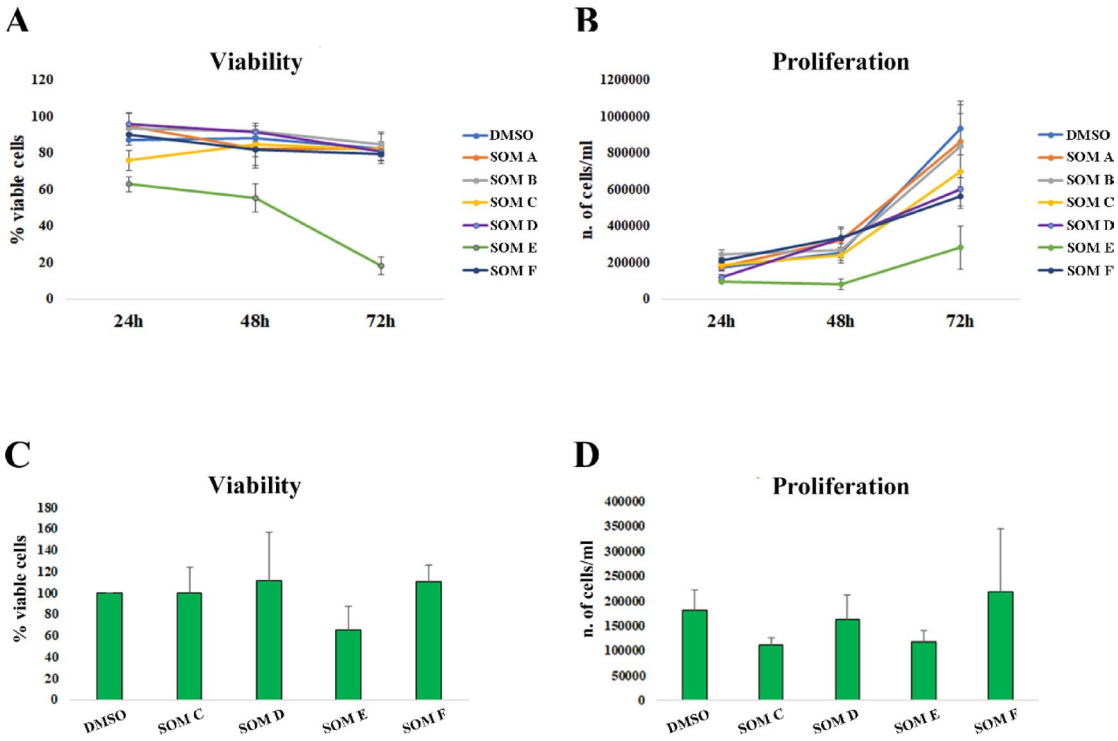

Fig. 2. Viability and proliferation analysis of OV90 cells after small organic molecules (SOMs) treatment. (**A**) Cell viability was assessed at 24, 48, 72 h by Trypan blue exclusion test using an automated cell counter. (**B**) Cell proliferation was assessed by counting the total number of cells at each time point, using an automated cell counter. Each condition was performed in quadruplicate. (**C**, **D**) same as A and B for DFs at 72 h. Data are expressed as mean ± SD. Statistical significance was determined using Student's t test by comparing each SOM-treated condition with DMSO at the corresponding time point. $^{*}p < 0.05$; $^{**}p < 0.01$; $^{***}p < 0.001$.

performed a western blotting analysis on OV90 cells treated for 72 h with SOMs C, D, and F. First, we analyzed the protein expression of GDF15, as a downstream of the mitochondrial Unfolded Protein Response. Both its precursor (pro-GDF15) and the mature form (m-GDF15) were detectable (Fig. 5A). We calculated the m-GDF15/pro-GDF15 ratio in order to have an indication of GDF15 processing. This ratio was significantly higher after treatment with SOM C (Fig. 5B). Then, we analyzed the protein expression of Grp78, a marker of endoplasmic reticulum stress, and of VDAC, a marker of mitochondrial mass. No significant variations of Grp78 levels were observed, following SOM treatments (Fig. 5A–C). Interestingly, amount upon GAPDH normalization, VDAC was significantly higher in cells treated with SOM D compared to DMSO-treated cells (Fig. 5A–D).

Finally, we tested the protein expression of representative subunits of the mitochondrial chain complexes. SOM D reduced the expression of Sdha and Cox IV, whereas SOM F reduced the expression of Sdha. No significant changes were observed in Ndufs1 and Uqcrc2 levels (Fig. 6A–E). These data suggest that SOM D, in particular, may cause an impairment of mitochondrial complexes assembly.

SOMs C and F increase ROS production in OV90 cells

Considering that SOMs C, D and F affected cell proliferation, gene and protein expression in OV90 cell line, we sought to verify if these molecules also affected glucose consumption and ROS production. To do so, we used two commercially available kits to assess, via a chemiluminescence reaction, glucose concentration and H_2O_2 production in OV90 cells, after a 72 h-treatment with the above-mentioned SOMs. Results were normalized over the total number of cells. SOMs C and D tended to increase glucose consumption, although not significantly (Fig. 7A). As far as ROS production, a small but significant increase in H_2O_2 production was observed in cells treated with SOMs C and F (Fig. 7B). Overall, these data indicate that SOMs C and F, but not D, could potentially affect the redox cellular balance.

Discussion

Elevated plasma levels of GDF15 have been associated with several pathologies, including T2D, cardiovascular, renal, and neurodegenerative diseases, as well as sarcopenia and frailty[9,25]. Therefore, the possibility to modulate GDF15 activity seems a potential treatment option for a number of disorders. Accordingly, GDF15 role in cancer cachexia is particularly well documented, and promising data on the use of moAbs against GDF15 in clinical trials with patients with advanced cancer have been recently reported[28,29]. In this study, we aimed to explore the possibility of applying an in silico screening methodology to discover commercially available SOMs potentially

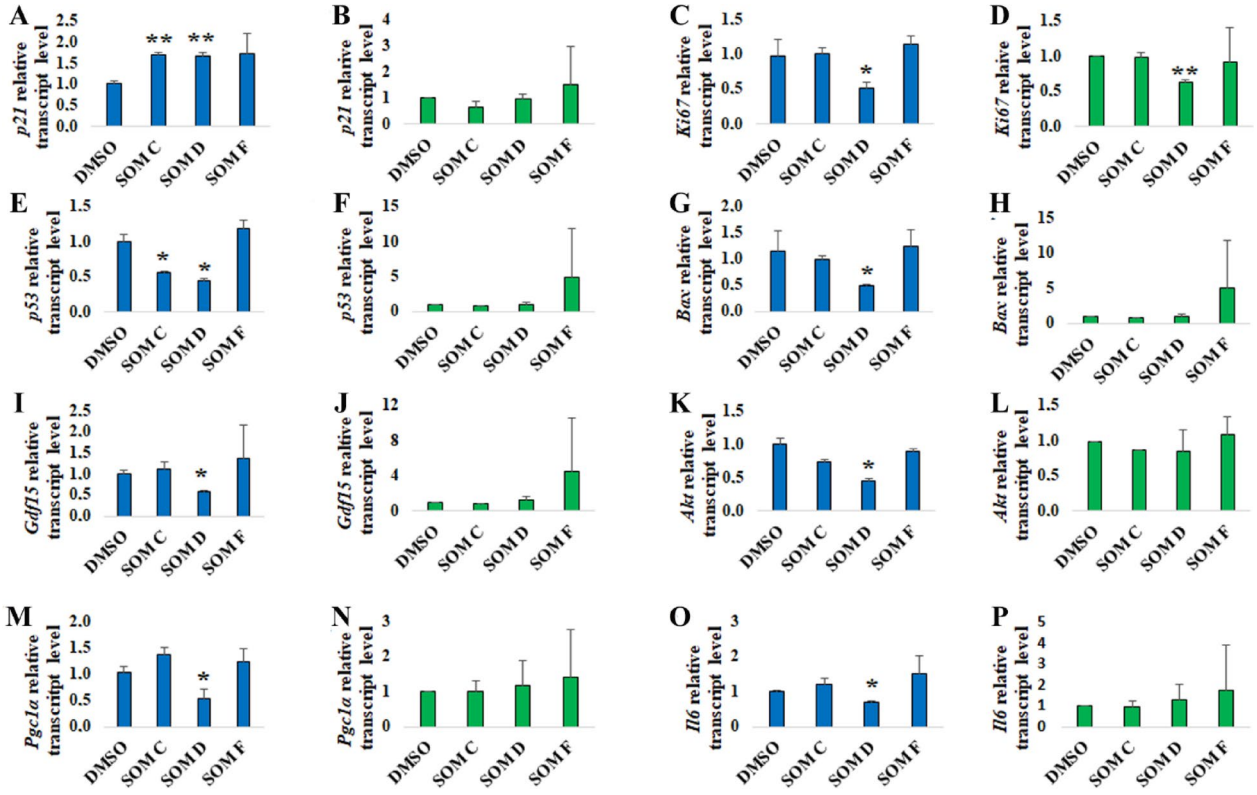

Fig. 3. Real time RT-PCR analysis in OV90 cells (blue columns) and DFs (green columns), after 72 h of treatment with small organic molecules (SOM C, D and F). (**A**, **B**) *p21*, (**C**, **D**) *Ki67*, (**E**, **F**) *p53*, (**G**, **H**) *Bax*, (**I**, **J**) *Gdf15*, (**K**, **L**) *Akt*, (**M**, **N**) *Pgc1a* and (**O**, **P**) *Il6* gene expression in 3 OV90 replicates and 2 DFs lines. Data are expressed as mean ± SD. Student's t test was applied to compare each small organic molecule (SOM C, D, F) treatment with respect to DMSO. $^{*}p < 0.05$; $^{**}p < 0.01$.

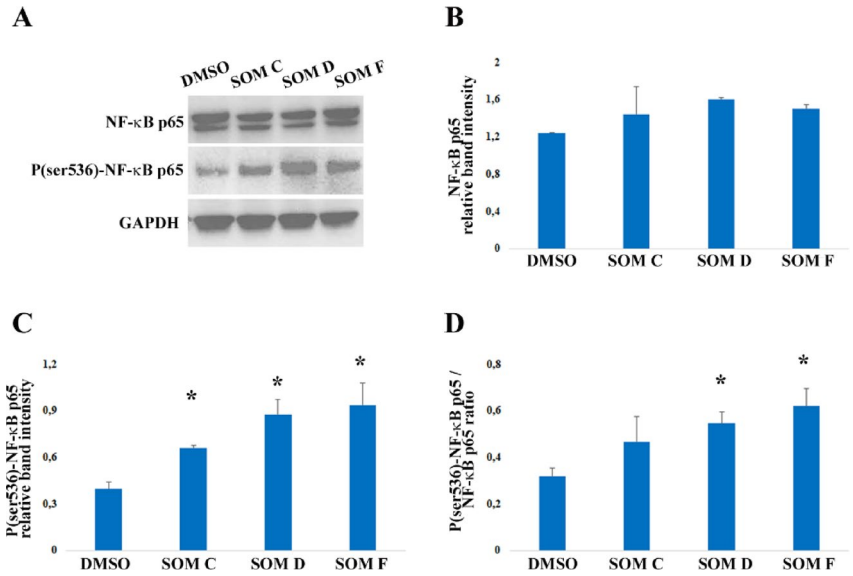

Fig. 4. Western blotting analysis of NF-κB p65 and phosphorylated NF-κB p65 (Ser536) in OV90 cells after 72 h of treatment with small organic molecules (SOM C, D and F). (**A**) Representative immunoblotting image; GAPDH was used as loading control. Relative band intensity of (**B**) NF-κB p65 and (**C**) phosphorylated NF-κB p65 (Ser536). (**D**) Ratio of phosphorylated NF-κB p65 (Ser536) to total NF-κB p65. Densitometric quantification was performed using Fiji software and normalized to GAPDH expression. Data are expressed as mean ± SD from 2 independent experiments. Student's t-test was applied to compare each SOM-treated condition with DMSO. $^{*}p < 0.05$.

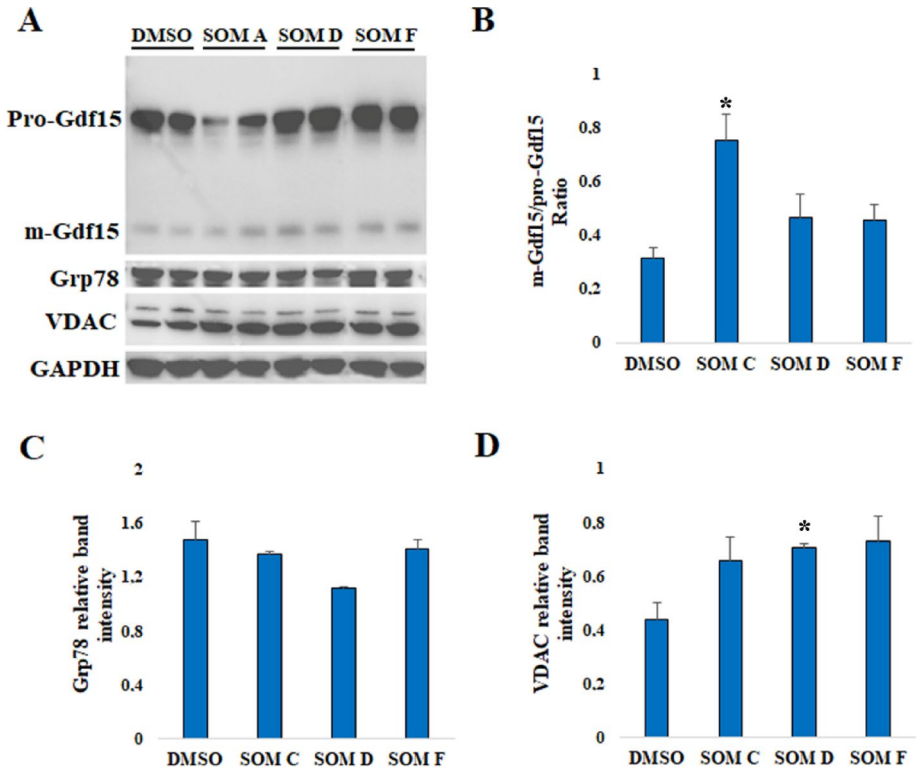

Fig. 5. Western blotting analysis of Gdf15, Grp78, VDAC and GAPDH in OV90 cells after 72 h of treatment with small organic molecules (SOM C, D and F). (**A**) Representative immunoblotting image of Gdf15 (m-Gdf15: mature form; pro-Gdf15: precursor form), Grp78, VDAC and GAPDH, used as loading control. (**B**) m-Gdf15/pro-Gdf15 ratio, based on m-Gdf15 and pro-Gdf15 relative band intensity. (**C**) Grp78 relative protein expression. (**D**) VDAC relative protein expression. Densitometric quantification was performed using Fiji software and normalized to GAPDH expression. Data are expressed as mean ± SD. Student's t-test was applied to compare each SOM-treated condition with DMSO. $^{*}p < 0.05$.

able to bind GDF15 in monomeric or dimeric form and modulate its biological effects, thus paving the way for a novel strategy for GDF15 inhibition.

Through this in silico screening we identified 6 SOMs, which appear to reduce GDF15 dimer stability, and four of them—SOMs C, D, E and F—also significantly decrease its binding to GFRAL. Because disulfide-linked oligomer readouts can be influenced by redox-active or thiol-reactive chemotypes, we cannot fully exclude assay-dependent or off-target contributions to the observed dimer-band changes. For this reason, we place greater interpretive weight on the purified-protein GDF15–GFRAL interaction assay; in this test, compounds were initially evaluated at 200 μM as a screening concentration to identify measurable modulation of the GDF15–GFRAL interaction. We acknowledge that this concentration does not establish potency or specificity and may increase the likelihood of non-specific effects. Accordingly, the results should be regarded as preliminary and motivate further optimization and quantitative characterization. Three out of four SOMs able to destabilize GDF15-GFRAL interaction were discovered through virtual screening performed on the dimeric structure of GDF15 (D, E, F), and their behavior can be explained by the location of their predicted binding site. Docking indicated that the molecules bind within a cavity at the interface of the two monomers, a region likely important for maintaining the dimer's overall shape and the conformation of the receptor-binding surface. Binding of SOMs in this pocket may cause local conformational adjustments that spread to the external parts of the dimer, slightly altering the geometry of the GFRAL-binding region and reducing receptor recognition. Because the screening was performed on a pre-assembled dimer, and even the less effective molecules (*e.g.*, SOM A and B) decreased dimer abundance, D, E, and F probably do not inhibit GDF15 by preventing dimerization. Instead, they seem to act as allosteric modulators: by occupying the inter-monomer cavity, they stabilize a dimeric form that remains structurally intact but is less compatible with GFRAL binding. This model may explain the reduced GDF15–GFRAL interaction, suggesting that these SOMs may function as allosteric antagonists.

No effects on cell viability were observed, except for SOM E that resulted acutely toxic, likely through mechanisms that go beyond GDF15 inhibition. For this reason, it was excluded from further testing. Proliferation was reduced in OV90 cells upon 72 h treatment with SOM D, F and (partially) C, while in DFs no effect was observed. This difference in the susceptibility to SOMs may be due to the different levels of GDF15 expressed by the two experimental models considered, and therefore to a different dependence on GDF15; however, other possible reasons cannot be ruled out, such as a different proliferation' rate of the two cell types. Further studies on a longer exposure time will be needed to exclude the presence of long-term effects on normal cells like DFs.

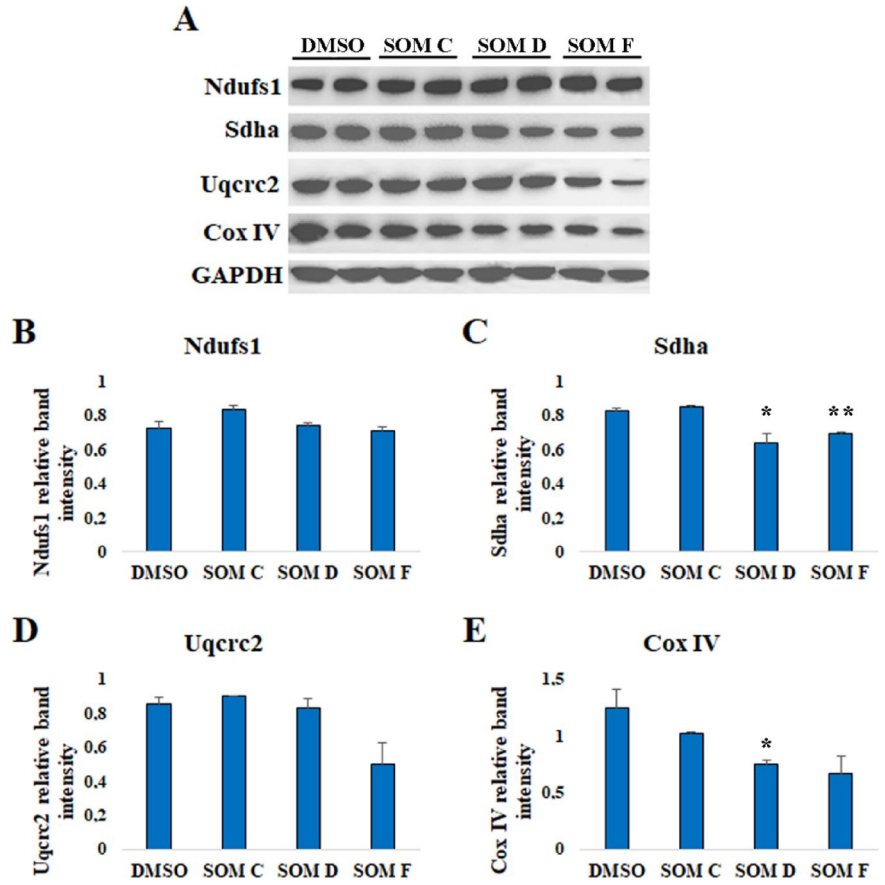

Fig. 6. Western blotting analysis of Ndufs1, Sdha, Uqcrc2 and Cox IV in OV90 cells after 72 h of treatment with small organic molecule (SOM C, D and F). (**A**) Representative immunoblotting image of Ndufs1, Sdha, Uqcrc2, Cox IV and GAPDH, used as loading control. Relative band intensity of (**B**) Ndufs1, (**C**) Sdha, (**D**) Uqcrc2 and (**E**) Cox IV. Data are expressed as mean ± SD. Student's t test was applied to compare each SOM-treated condition with DMSO. $*p < 0.05$, $**p < 0.01$. Densitometric quantification was performed using Fiji software and normalized to GAPDH expression.

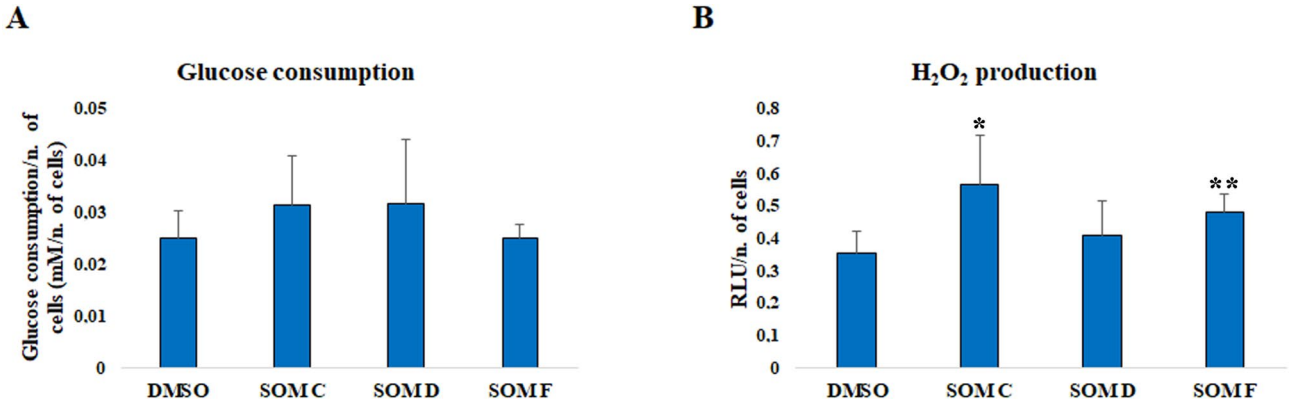

Fig. 7. Functional assays on OV90 cells. (**A**) Glucose consumption and (**B**) ROS (H_2O_2) production were analyzed by chemiluminescent assays following treatment with the small organic molecules (SOM C, D and F). Glucose consumption is expressed as the difference between the initial glucose concentration (mM) in the culture medium, and the concentration at the end of the treatment. This value is normalized to the total number of cells. H_2O_2 production is expressed as relative light units (RLU) per cell. Data are expressed as mean ± SD from two independent experiments, each performed in triplicate. Student's t test was applied to compare each SOM-treated condition with DMSO. * $p > 0.05$; ** $p > 0.01$.

Although additional biophysical assays (*e.g.*, SPR/ITC/thermal shift) would further strengthen target-engagement claims, these approaches require substantial assay optimization and are sensitive to compound solubility/aggregation and surface artefacts. Accordingly, we interpret our current data as evidence that SOMs C, D and F can modulate the GDF15–GFRAL interaction in a purified-protein acellular assay consistent with engagement of the GDF15 system. To further substantiate this hypothesis, we have performed expression analysis of some genes. While the analysis of *p21* and *Ki67* genes corroborated the proliferation analysis, the results of other genes like *Pgc1α* and *Il6* that are *bona fide* downstream target of GDF15 signaling pathway[20,37] support the hypothesis that these molecules, in particular SOM D can at least in part modulate GDF15 biological activity. Once again, the effects on gene expression were mostly visible in OV90 cells rather than DFs. GDF15 can block NF-κB protein activation[16], and accordingly p65 phosphorylation resulted increased upon treatment with SOM D and F, further supporting our conclusions.

Mitochondria appear impaired upon SOM D treatment (mass is increased, while biogenesis is likely altered as *Pgc1*α, *Sdha*, and *Cox IV* expression are decreased); however, H_2O_2 production and glucose consumption are unaffected. At variance, SOM C and F caused an apparently smaller effect on mitochondrial subunit expression but a significant increase in H_2O_2 production. Since all these three SOMs cause a decrease in proliferation (although just as a trend for SOM C), it is likely that this is linked to an effect on mitochondrial function for SOM C and F but not SOM D, which appears to be linked to increased *p21* and decreased *Ki67* expression. Previous report has linked GDF15 to cell senescence[38]. Accordingly, SOM D appears to affect proliferation much more than mitochondrial function. Interestingly, the effects are seen primarily in OV90 cancer cells that express high levels of GDF15; almost nothing is observed in normal cells such as DFs. All the above cell-based readouts are presented as supportive observations consistent with modulation of GDF15 activity; however, without quantitative target-engagement measurements we cannot exclude secondary mechanisms.

We have no indication whether these SOMs (especially D) have an anticachectic effect, for which data from in vivo models would be needed; moreover, establishing relevance to anorexia/cachexia or inflammatory phenotypes will require optimization of the candidate molecule to sub-micromolar potency and appropriate pharmacokinetics, followed by pathway- and physiology-level assays, which are beyond the scope of the present proof-of-concept study. Nevertheless, we do have an interesting indication on which cells, normal or cancer ones, are more affected by inhibition of GDF15 signaling. In particular, according to our data, cells like DFs do not appear to be significantly affected by treatment with SOMs at these doses and times, unlike tumor OV90 cells, which increase the expression of senescence markers such as p21 and decrease the expression of GDF15 itself. This suggests that the use of SOMs against GDF15 at the cellular level should be non-toxic for normal cells, also in agreement with what was observed in clinical trials with anti-GDF15 moAbs, where no increase in side effects was recorded in the treated patient group compared to the placebo group[28].

Overall, SOM D (corresponding to vendor's code Z771945868) displays the most prominent and congruent results for being a promising candidate molecule for the inhibition of GDF15 activity. To our knowledge, this is the first reported small-molecule scaffold that modulates the GDF15 activity in both acellular and cellular assays. Other SOMs exhibited either partial activity or significant toxicity, indicating a different mechanism of action other than GDF15 signaling inhibition.

Limitations and future work: this study has several limitations that should be considered when interpreting the results and defining next research steps. First, the structure-based screening and docking workflow identifies candidates with plausible binding modes; however, docking scores and predicted poses remain qualitative and require experimental corroboration. Second, although the GDF15–GFRAL protein–protein interaction assay is a target-proximal functional experiment performed on purified components, it does not by itself yield quantitative binding constants and cannot fully exclude alternative mechanisms such as interaction with the receptor components or non-specific effects at high compound concentrations. Future work will therefore prioritize (i) quantitative biophysical characterization of compound engagement (*e.g.*, using orthogonal binding and stability approaches, coupled with appropriate counterscreens), (ii) expansion of structure–activity relationships through analog testing to improve potency and physicochemical behavior, and (iii) further mechanistic interrogation in cellular systems using concentration–response designs. Collectively, these efforts will consolidate the on-target mechanism and support rational optimization of SOM D as a chemical probe for the modulation of GDF15 activity.

Data availability

Most of the data generated during this study are included in this article (and its Supplementary Data files). Any other information about analysis are available from the corresponding author on reasonable request.

Received: 8 January 2026; Accepted: 30 April 2026
Published online: 07 May 2026

References

1. Bootcov, M. R. et al. MIC-1, a novel macrophage inhibitory cytokine, is a divergent member of the TGF-beta superfamily. *Proc. Natl. Acad. Sci. U S A* **94**, 11514–11519 (1997).
2. Hromas, R. et al. PLAB, a novel placental bone morphogenetic protein. *Biochim. Biophys. Acta* **1354**, 40–44 (1997).
3. Lawton, L. N. et al. Identification of a novel member of the TGF-beta superfamily highly expressed in human placenta. *Gene* **203**, 17–26 (1997).
4. Durieux, J., Wolff, S. & Dillin, A. The cell-non-autonomous nature of electron transport chain-mediated longevity. *Cell* **144**, 79–91 (2011).
5. Breit, S. N., Brown, D. A. & Tsai, V. W. The GDF15-GFRAL pathway in health and metabolic disease: Friend or foe?. *Annu. Rev. Physiol.* **83**, 127–151 (2021).
6. Tanaka, T. et al. Plasma proteomic signature of age in healthy humans. *Aging Cell* **17**, e12799 (2018).

7. Conte, M. et al. Human aging and longevity are characterized by high levels of mitokines. *J. Gerontol. A Biol. Sci. Med. Sci.* **74**, 600–607 (2019).
8. Conte, M. et al. GDF15, an emerging key player in human aging. *Ageing Res. Rev.* **75**, 101569 (2022).
9. Wan, Y. & Fu, J. GDF15 as a key disease target and biomarker: Linking chronic lung diseases and ageing. *Mol. Cell. Biochem.* **479**, 453–466 (2024).
10. Emmerson, P. J. et al. The metabolic effects of GDF15 are mediated by the orphan receptor GFRAL. *Nat. Med.* **23**, 1215–1219 (2017).
11. Hsu, J. Y. et al. Non-homeostatic body weight regulation through a brainstem-restricted receptor for GDF15. *Nature* **550**, 255–259 (2017).
12. Mullican, S. E. et al. GFRAL is the receptor for GDF15 and the ligand promotes weight loss in mice and nonhuman primates. *Nat. Med.* **23**, 1150–1157 (2017).
13. Yang, L. et al. GFRAL is the receptor for GDF15 and is required for the anti-obesity effects of the ligand. *Nat. Med.* **23**, 1158–1166 (2017).
14. Wang, W. et al. Prostate cancer promotes a vicious cycle of bone metastasis progression through inducing osteocytes to secrete GDF15 that stimulates prostate cancer growth and invasion. *Oncogene* **38**, 4540–4559 (2019).
15. Takahashi, M. RET receptor signaling: Function in development, metabolic disease, and cancer. *Proc. Jpn. Acad. Ser. B Phys. Biol. Sci.* **98**, 112–125 (2022).
16. Lambert, J. R. et al. Reduced expression of GDF-15 is associated with atrophic inflammatory lesions of the prostate. *Prostate* **75**, 255 (2015).
17. Hüllwegen, M., Kleinert, M., von Haehling, S. & Fischer, A. GDF15: From biomarker to target in cancer cachexia. *Trends Cancer* **11**, 1093–1105 (2025).
18. Luan, H. H. et al. GDF15 is an inflammation-induced central mediator of tissue tolerance. *Cell* **178**, 1231-1244.e11 (2019).
19. Bonaterra, G. A. et al. Growth differentiation factor-15 deficiency inhibits atherosclerosis progression by regulating interleukin-6-dependent inflammatory response to vascular injury. *J. Am. Heart Assoc.* **1**, e002550 (2012).
20. Tsui, K. H. et al. Growth differentiation factor-15 upregulates interleukin-6 to promote tumorigenesis of prostate carcinoma PC-3 cells. *J. Mol. Endocrinol.* **49**, 153 (2012).
21. Di Micco, R., Krizhanovsky, V., Baker, D. & d'Adda di Fagagna, F. Cellular senescence in ageing: From mechanisms to therapeutic opportunities. *Nat. Rev. Mol. Cell Biol.* **22**, 75–95 (2021).
22. Jin, Y. J., Lee, J. H., Kim, Y. M., Oh, G. T. & Lee, H. Macrophage inhibitory cytokine-1 stimulates proliferation of human umbilical vein endothelial cells by up-regulating cyclins D1 and E through the PI3K/Akt-, ERK-, and JNK-dependent AP-1 and E2F activation signaling pathways. *Cell. Signal.* **24**, 1485–1495 (2012).
23. Chiariello, A. et al. The expression pattern of GDF15 in human brain changes during aging and in Alzheimer's disease. *Front. Aging Neurosci.* **14**, 1058665 (2023).
24. Chiariello, A. et al. Different roles of circulating and intramuscular GDF15 as markers of skeletal muscle health. *Front. Endocrinol. (Lausanne)* **15**, 1404047 (2024).
25. Conte, M. et al. The combination of GDF15, FGF21, sRAGE and NfL plasma levels can identify frailty in community-dwelling people across old age. *Mech. Ageing Dev.* **226**, 112077 (2025).
26. Siddiqui, J. A. et al. Pathophysiological role of growth differentiation factor 15 (GDF15) in obesity, cancer, and cachexia. *Cytokine Growth Factor Rev.* **64**, 71–83 (2022).
27. Wang, D. et al. GDF15 promotes weight loss by enhancing energy expenditure in muscle. *Nature* **619**, 143–150 (2023).
28. Groarke, J. D. et al. Ponsegromab for the treatment of cancer cachexia. *N. Engl. J. Med.* **391**, 2291–2303 (2024).
29. Melero, I. et al. Neutralizing GDF-15 can overcome anti-PD-1 and anti-PD-L1 resistance in solid tumours. *Nature* **637**, 1218–1227 (2025).
30. Alexopoulou, F. et al. Identification of GDF15 peptide fragments inhibiting GFRAL receptor signaling. *Peptides* **168**, 171063 (2023).
31. Borner, T. et al. Creation of a peptide antagonist of the GFRAL-RET receptor complex for the treatment of GDF15-induced malaise. *J. Med. Chem.* **66**, 11237–11249 (2023).
32. Noisier, A. F. M. et al. Design of bicyclic peptide tandems mimicking the homodimeric GDF15 PROTEIN TO INHIBIT GDF15-GFRaL-RET complex cell signaling. *J. Med. Chem.* **68**, 21441–21457 (2025).
33. Polák, L. et al. PrankWeb 4: A modular web server for protein–ligand binding site prediction and downstream analysis. *Nucleic Acids Res.* **53**, W466–W471 (2025).
34. Trott, O. & Olson, A. J. AutoDock Vina: Improving the speed and accuracy of docking with a new scoring function, efficient optimization, and multithreading. *J. Comput. Chem.* **31**, 455–461 (2010).
35. Eberhardt, J., Santos-Martins, D., Tillack, A. F. & Forli, S. AutoDock Vina 1.2.0: New docking methods, expanded force field, and Python bindings. *J. Chem. Inf. Model.* **61**, 3891–3898 (2021).
36. Osada, M. et al. A p53-type response element in the GDF15 promoter confers high specificity for p53 activation. *Biochem. Biophys. Res. Commun.* **354**, 913–918 (2007).
37. Aguilar-Recarte, D. et al. A positive feedback loop between AMPK and GDF15 promotes metformin antidiabetic effects. *Pharmacol. Res.* **187**, 106578 (2023).
38. Chiariello, A. et al. Downregulation of PLIN2 in human dermal fibroblasts impairs mitochondrial function in an age-dependent fashion and induces cell senescence via GDF15. *Aging Cell* **23**, e14111 (2024).

Author contributions

AC performed and designed experiments, maintained cell cultures, performed statistical analyses and wrote the manuscript. LT maintained cell cultures and performed Real Time PCR analyses. MS and ML critically discussed the results. ADR, LL and MDP performed in silico analysis and provided SOMs. SS and MC carried out the design of the study, critically analyzed the results, and wrote the manuscript. All authors contributed to the article and approved the submitted version.

Funding

The work was co-funded from the Italian Ministry of University and Research (MUR) PRIN 2022, Project # 2022KS8T4N "GDF15 as a key player and a potential target to tackle ageing and age-associated diseases: an in silico, in vitro and ex vivo study" to SS and MDP. The work was also co-funded from Next Generation EU, in the context of the National Recovery and Resilience Plan, Investment PE8—Project Age-It: "Ageing Well in an Ageing Society" to SS. This resource was co-financed by the Next Generation EU [DM 1557 11.10.2022]. The research leading to these results has received funding by the Italian Ministry of Health, RC-2025-2794605. The views and opinions expressed are only those of the authors and do not necessarily reflect those of the European Union or the European Commission. Neither the European Union nor the European Commission can be held

responsible for them.

Declarations

Competing interests
The authors declare no competing interests.

Consent for publication
All authors have given their consent to publish.

Additional information
Supplementary Information The online version contains supplementary material available at https://doi.org/10.1038/s41598-026-51932-x.

Correspondence and requests for materials should be addressed to S.S.

Reprints and permissions information is available at www.nature.com/reprints.

Publisher's note Springer Nature remains neutral with regard to jurisdictional claims in published maps and institutional affiliations.